Case Studies in Construction Materials 25 (2026) e06507

Contents lists available at ScienceDirect

Case Studies in Construction Materials

journal homepage: www.elsevier.com/locate/cscm

A data-driven framework for mix design optimization of limestone calcined clay cement concrete using machine learning and experimental validation

Md Rakib Hossain [a], Jawad Khalil [a], Amin Al-Fakih [a,b,*], Fahd Saeed Alakbari [c], Abdullah Alshahrani [d,e], Ayman Almutlaqah [d,f,**]

[a] Department of Civil and Environmental Engineering, King Fahd University of Petroleum & Minerals, Dhahran 31261, Saudi Arabia
[b] Interdisciplinary research Center for Construction and Building Materials, King Fahd University of Petroleum & Minerals, Dhahran 31261, Saudi Arabia
[c] Interdisciplinary Research Center for Hydrogen Technologies and Carbon Management, King Fahd University of Petroleum & Minerals, Dhahran 31261, Saudi Arabia
[d] Civil Engineering Department, College of Engineering, Najran University, Najran, Saudi Arabia
[e] Science and Engineering Research Center, Najran University, Najran, Saudi Arabia
[f] School of Engineering, Cardiff University, Cardiff CF24 3AA, United Kingdom

A R T I C L E I N F O

Keywords:
LC^3
Machine learning
Greywolf optimization
CatBoost
Compressive strength
Sustainability

A B S T R A C T

Limestone calcined clay cement (LC^3) offers a promising binder for reducing clinker in concrete; however, its compressive strength is influenced by both binder chemistry and mix proportions. Although many studies have investigated LC^3, an integrated approach that combines machine learning prediction, optimization, and experimental validation for mix design is still limited. This study proposes a metaheuristic-assisted machine learning based framework to predict the compressive strength of LC^3 concrete, and to identify an optimal mix design. The optimized mix was then subjected to preliminary experimental validation. A literature database of 172 LC^3 concrete mixtures compiled from 42 published studies was used, with 19 input variables describing oxide compositions of Ordinary Portland cement (OPC), calcined clay (CC), and limestone powder (LSP), together with key mix parameters. Four ensemble learners (CatBoost, XGBoost, Random Forest, and LightGBM) were trained using an 80/20 train–test split. Five-fold cross-validation was applied to ensure model reliability. CatBoost provided the best generalization on the test set compared to other models studied. SHAP results revealed that the water-to-binder ratio (W/B) was the most important factor in determining strength, followed by the content of coarse aggregate (CA) content, sand-to-binder ratio (S/B), and LSP content. The trained CatBoost model was coupled with a Gray Wolf Optimizer (GWO) to obtain a feasible optimal combination. The strength was predicted to be 57.21 MPa. The average strength of 100 mm cubes was 51.54 MPa with standard deviation of 0.21 MPa. The proposed framework has the potential to be used for data-driven design of LC^3 concretes.

* Corresponding author at: Department of Civil and Environmental Engineering, King Fahd University of Petroleum & Minerals, Dhahran 31261, Saudi Arabia
** Corresponding author at: Civil Engineering Department, College of Engineering, Najran University, Najran, Saudi Arabia
E-mail addresses: aminali.fakih@kfupm.edu.sa (A. Al-Fakih), almutlaqahAA1@cardiff.ac.uk (A. Almutlaqah).

https://doi.org/10.1016/j.cscm.2026.e06507
Received 29 June 2026; Received in revised form 24 August 2026; Accepted 5 September 2026
Available online 6 September 2026
2214-5095/

1. Introduction

Urbanization and infrastructure development activities are expected to drive global demand for concrete to 6 billion tonnes by 2060 [1]. Ordinary Portland cement (OPC) is energy-intensive and produces 8% of CO2 emissions in the atmosphere as a result of its use as a binder in concrete mixtures. Moreover, the cement and concrete sector accounts for nearly 39% of energy-related industrial emissions [2]. These figures underscore the urgent need to decarbonize cementitious systems in alignment with international climate mitigation targets. In OPC, it was found that the major contributor to CO_2 emissions is clinker production. It is a result of both fuel combustion and calcination of limestone. Hence, using alternative materials in partial replacement of clinker can be a good option for reducing embodied carbon. LC^3 is a newly found alternative cement for reducing CO_2 emissions. It is a quaternary cement containing clinker, calcined clay (CC), limestone powder (LSP), and gypsum (GYP) [3]. LC^3 composition can minimize the clinker content by up to 50%, resulting 30–40% decrease in CO_2 emissions compare to conventional OPC. CC is typically produced at moderate temperatures (700–800 °C), significantly lower than those required for clinker production, and does not involve process emissions from carbonate decomposition [4]. Previous studies have reported that LC^3-50 mixes comprise 50% clinker, 30% CC, 15% LSP and 5% GYP. These mixes achieve comparable compressive strengths to OPC in 28-days, which supports their potential use as low-carbon binders in structural applications [5]. In the case of LC^3 mortars with 65% clinker content (LC^3-65), where waste brick powder was used in place of CC. The resulting compressive strength was comparable to the reference mixture. The mixtures preserved approximately 98% of the reference strength at 7 days and 93% at 28 days [2]. For LC^3-50, the loss of strength was more apparent; nevertheless, the strength values were still within the required limits of minimum strength. The large-scale life-cycle assessment's findings show that substitution of 50% of the clinker content with a metakaolin-limestone blend can lead to a substantial reduction in environmental impact. This method reduces greenhouse gas (GHG) emissions by about 30% and the production costs by 12% [6].

Nevertheless, LC^3 concrete's growing popularity necessitates effective tools for designing and predicting mix performance. Compressive strength (CS) continues to be one of the prime properties for determining whether concrete mixes are suitable for structural applications [7–9]. But laboratory testing is slow when a number of variables influence strength, including binder proportions, water-to-binder ratio (W/B ratio), curing, aggregate characteristics, and chemical admixtures [10]. In LC^3 systems, prediction is even more challenging because hydration chemistry is complex and depends strongly on clay quality and reactivity. Conventional analytical or empirical models may not capture these interactions well, and developing LC^3-specific models remains difficult [11]. Therefore, there is growing interest in data-driven approaches that can learn these relationships from existing data.

Machine learning (ML) is acknowledged as a powerful approach for estimating properties of concrete because of its capacity to capture the nonlinear relationships among a number of factors. ML models can recognize patterns, and interactions which is challenging to depict using conventional equations by training on experimental data [12]. Machine learning approaches have been used to systems based on CC and LC^3 . Drawing from paste and mortar data, Han et al. (2023) developed a Random Forest model and obtained an R^2 value of approximately 0.92 for predicting compressive strength, but only through prediction rather than for mixture optimization or for the validation of optimized mixtures [13]. In order to reduce cost and carbon footprint, Chen et al. (2025) created a hybrid ML and multi-objective optimization technique for LC^3 concrete and used a MICE-XGBoost model integrated with NSGA-II to achieve a R^2 value of 0.928. However, the optimized mixes were not tested [14]. By combining ML with metaheuristic optimization, Sapkota et al. (2025) were able to reach R^2 values greater than 0.97; however, their optimization focused on model parameters rather than particular mix designs [11]. Liu et al. (2025) investigated LC^3 -ECCs and reached an R^2 of 0.977 with optimized XGBoost models, but their interest was in ECCs, not conventional LC^3 concrete, and no experimental validation of optimized mix designs was carried out [15]. Canbek et al. (2022) determined the yield stress rather than compressive strength when predicting the rheological properties of LC^3 pastes, with an R^2 of 0.967 [16]. Similarly, Bansal et al. (2022) combined ML with embedded sensor monitoring in LC^3 paste system to achieve R^2 values close to 0.99; however, their study was restricted to paste systems and did not address the mix optimization [17]. In general, most existing studies focus mainly on improving prediction accuracy. Only a very small number of studies attempt mix optimization, and even in those cases the optimized mixtures are not validated through laboratory testing at the concrete level.

In addition to LC^3-specific studies, recent research has also integrated machine learning and metaheuristic algorithms in construction and structural engineering. For instance, Zhang et al. (2026) introduced a metaheuristic-based framework called CatBoost to predict the mechanical properties of corroded reinforced concrete beams [18]. Model interpretation was also employed to interpret the predictions. The use of machine learning, metaheuristic optimization and model interpretation is shown to be helpful for a complex engineering problem. The purpose of the use of a metaheuristic algorithm, however, can be different. These can be used to fine-tune the parameters of ML models, or to identify an optimum engineering design with a trained ML model. The present study follows the second approach. CatBoost is used as the prediction model and GWO to find feasible LC^3 concrete mix proportions based on the predicted compressive strength. The best mixture is then tested in the laboratory.

Despite the significant contributions of these studies toward the comprehension of LC^3 and the application of ML methods, it can be noted that the scope and goals of these studies are vastly different from those of the current investigation. Table 1 shows the significant differences between existing LC^3 ML research and the current investigation with respect to material type, modeling approach, optimization method, and experimental validation.

As seen in Table 1, most current LC^3-related ML studies have been limited to primarily property prediction. The application of ML to optimization has been explored in very limited studies, and experimental validation of optimized LC^3 concrete mixtures is limited. Hence, the major contribution of the current study is based on these following novel aspects: integration of multiple ML models; interpretation using SHAP; mix design optimization utilizing GWO and laboratory validation.

Table 1
Comparison of existing LC^3 –ML studies with the present study.

Ref.	LC^3 form	ML models	ML application	Difference from current study
[14]	LC^3 Concrete (387 samples; paste + mortar + concrete)	MICE-XGBoost + NSGA-II	Prediction of compressive strength + multi-objective optimization	No experimental validation of optimized mix
[13]	LC^3 (Paste + Mortar, 430 samples)	Random Forest	Prediction of compressive strength only	No mix optimization; no experimental validation
[17]	LC^3 Paste	ANN, ML regression	Prediction of compressive strength only	Paste only; no mix optimization
[15]	LC^3-ECC (156 samples)	MH-XGBoost, GEP	Prediction of compressive strength + hyperparameter optimization	Optimization for model tuning only; no experimental validation
[16]	LC^3 Paste	ML regression	Rheology prediction only	Focus on yield stress; no strength optimization
[19]	LC^3 mortar	RF, GBM, ET, XGBoost, and CatBoost	Compressive strength prediction only	No experimental validation
[20]	LC^3 Concrete	RF-PO + XGB-LS	Compressive strength prediction + hyperparameter optimization	No experimental validation
[21]	LC^3 Mortar	ANN, SVM	Compressive strength prediction only	Mortar only, and also no optimization and lab validation
[22]	Low-carbon cementitious materials	Interpretable ML models	Autogenous shrinkage prediction only	ML used to optimize autogenous shrinkage properties, not compressive strength
Current Study	LC^3 Concrete	XGBoost, RF, CatBoost, LightGBM, Greywolf optimization	Compressive strength prediction + Greywolf optimization for mix design, and SHAP	LC^3 concrete-specific, multiple ML models for robustness, Compressive strength prediction, Mix design optimization, preliminary experimental validation

2. Methodology and data description

2.1. Methodology

Fig. 1 presents the complete methodological process followed in this research. This starts with data collection, followed by data preprocessing, and exploratory data analysis to assess quality and consistency of the data. The data is then divided into a training set (80%) and a testing set (20%) for model development and evaluation. GridSearchCV-based hyperparameter tweaking is used to improve the performance of several algorithms that are tested using five-fold cross-validation during model training. If the model's performance falls short of the necessary accuracy, the tuning procedure is repeated until a suitable result is obtained. Following training, the model is evaluated on testing set, and the performance is judged based on the determination coefficient ($R^2 \geq 0.8$), RMSE, MAE, and MSE metrics. The best model is then selected and combined with GWO technique to determine the optimum LC^3 mix proportions for maximum compressive strength. Finally, the optimized mix design was subjected to preliminary experimental validation through laboratory testing. This validation was used as a case study to compare the model prediction with the measured 28-day compressive strength.

2.2. Data collection

The compiled dataset, which includes 172 datapoints from 42 published research articles from 2015 to 2025 [7,23–63], which were used to develop the ML models. To achieve the homogeneity, these studies were selected based on their suitability for LC^3 concrete mixes rather than for LC^3 mortar or paste systems. The input features were selected to represent both raw-material chemistry and concrete mix proportions. The chemical compositions of the OPC, CC, and LSP were also included to reflect the diversity of their

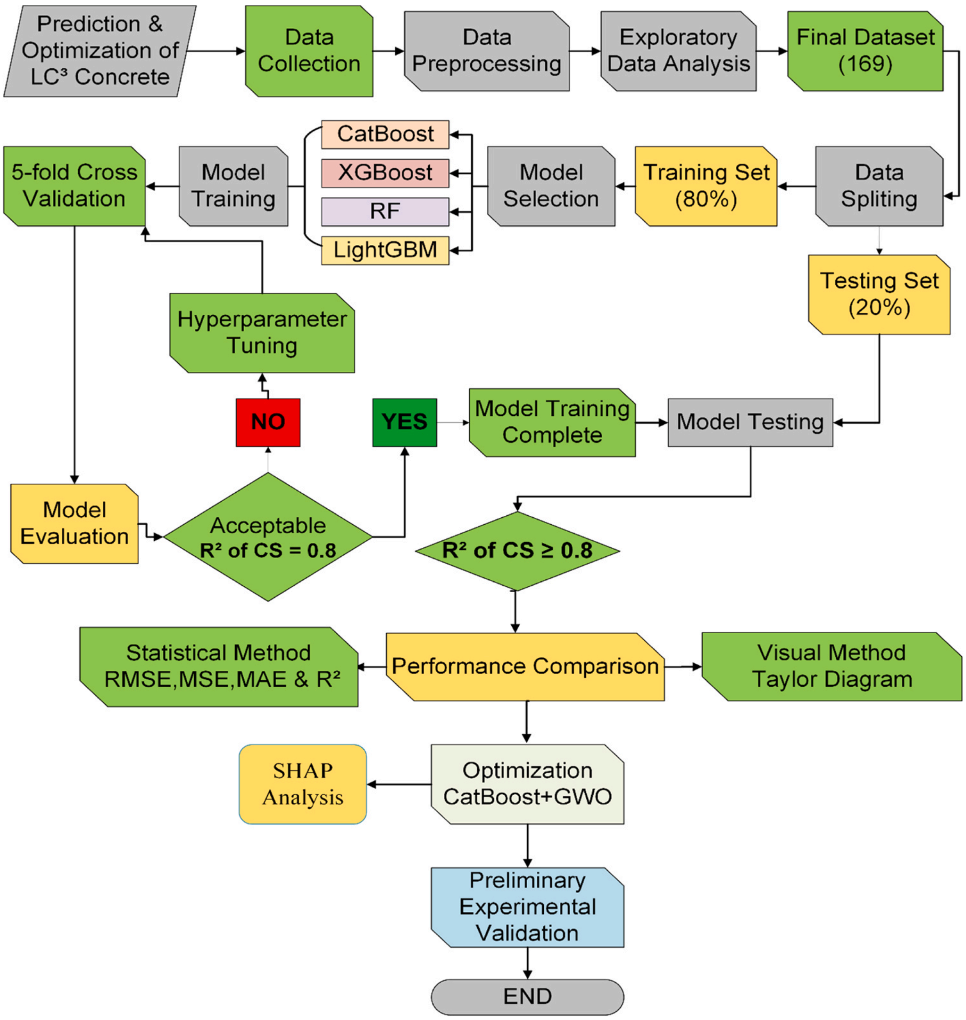

Fig. 1. Methodological workflow.

chemical properties reported in various studies. These differences may impact the hydration and strength development of LC^3 systems. The other variables, such as binder content, OPC, CC, LSP, GYP, aggregate contents, S/B ratio and W/B ratio are the main proportions of the concrete mixture. So, the selected features enable the ML models to take the material-related and mix design-related effects on CS into consideration. Statistical analyses of the variables are presented in Table 2.

2.3. Data preprocessing

The initial dataset contained 172 observations. The dataset was checked for missing values, duplicate observations, non-numeric entries, and formatting errors. No missing values were identified; therefore, no imputation was required. Three duplicate observations were identified and removed, resulting in a final dataset of 169 observations. The input features were then separated from the target variable, which was the 28-day compressive strength. No automatic statistical outlier-removal method was applied. Extreme observations were retained when they were physically plausible because the dataset was compiled from different LC^3 concrete studies with wide variations in material chemistry and mix proportions. For example, the W/B ratio ranged from 0.25 to 0.60, while the 28-day compressive strength ranged from 14.84 to 77.91 MPa. Retaining these observations preserved the experimental variability represented in the literature database. The final dataset was divided into training and testing sets using an 80/20 split. This ratio was selected to retain most of the observations for model development while preserving an independent subset for final evaluation. Approximately 135 observations were used for training and 34 observations were reserved for testing. A fixed random seed (random_state = 42) was used only to ensure reproducibility of the data partition and to provide the same training and testing samples for all four ML models. The value 42 has no specific statistical advantage. Five-fold cross-validation within GridSearchCV was applied to the training data for model selection and hyperparameter tuning, while the independent test set remained unused until the final model evaluation. No data augmentation or synthetic data generation was applied in the present study. All observations used for model development and evaluation were experimentally reported LC^3 concrete data collected from the literature.

2.4. Correlation heatmap analysis

Fig. 2 is the heatmap correlation for the input variables and CS_28 for LC^3 concretes. The correlation coefficient for LC^3 binder content is 0.46, indicating a moderate relationship between both strength and binder content. OPC content ($r = 0.19$) and the S/B ratio ($r = 0.23$) present weak-to-moderate positive relations as well, indicating that adequate binder content and well-graded aggregate induce excellent compressive performance. On the other hand, water-to-binder ratio exhibited a weak negative correlation (-0.18), a finding that supported the fact that higher water volume increases porosity, consequently reducing strength. The chemical constituents showed that CaO in OPC and CaO in LSP produced small positive effects of 0.19 and 0.05, respectively, while Fe_2O_3 in CC had a small -0.26, likely owing to its insignificant role in hydration. Of note, SiO_2 and Al_2O_3 in CC are associated with 0.65 with consistent composition in clay sources, while CaO and Al_2O_3 in OPC are moderately associated with 0.64 indicating associated clinker variation. Overall, these correlations confirm that LC^3 concrete strength is controlled by a number of combined binder chemistry, mix proportions, and water content rather than any single parameter; thus, more complex machine learning approaches are required, capable of handling nonlinear interactions.

Table 2
Statistical analysis of the raw dataset.

Parameters	count	mean	std	min	25%	50%	75%	max
CC(SiO2)%	169.0	57.96	7.35	35.64	54.67	54.67	60.61	78.71
CC(Al2O3)%	169.0	29.31	6.85	12.37	24.95	27.69	29.72	46.96
CC(Fe2O3)%	169.0	3.69	2.5	0.18	1.95	4.93	4.93	15.38
CC(CaO)%	169.0	0.52	0.81	0.01	0.06	0.09	1.08	5.69
OPC(SiO2)%	169.0	20.11	1.28	15.41	19.01	20.10	21.12	23.52
OPC(Al2O3)%	169.0	4.59	0.65	3.51	4.17	4.40	5.10	7.16
OPC(Fe2O3)%	169.0	3.54	0.88	2.00	2.92	3.58	3.89	5.60
OPC(CaO)%	169.0	63.75	1.83	55.94	63.17	63.81	64.59	69.86
LSP(Si02)%	169.0	8.58	7.94	0.10	0.57	10.07	11.25	27.01
LSP(CaO)%	169.0	54.04	19.31	31.50	44.24	48.54	55.00	98.72
LC^3 binder (Kg/m^3)	169.00	406.18	61.31	291.00	360.00	400.00	420.00	700.00
CC (%)	169.00	27.68	7.07	6.50	22.10	30.00	30.00	45.00
OPC(%)	169.00	56.07	12.27	30.00	50.00	55.00	70.00	90.00
GYP (%)	169.00	1.66	2.10	0.00	0.00	0.00	4.00	10.00
LSP(%)	169.00	14.59	7.86	3.30	10.00	15.00	15.00	49.00
S/B ratio	169.00	2.05	0.49	1.10	1.66	2.11	2.37	3.28
CA (kg/m^3)	169.00	1001.87	142.78	600.00	894.00	994.10	1098.00	1540.00
FA (kg/m^3)	169.00	812.62	141.68	575.00	687.00	842.40	909.50	1200.00
W/B ratio	169.00	0.41	0.069	0.25	0.40	0.40	0.46	0.60
CS_28	169.00	47.77	13.10	14.84	38.40	47.50	56.87	77.91

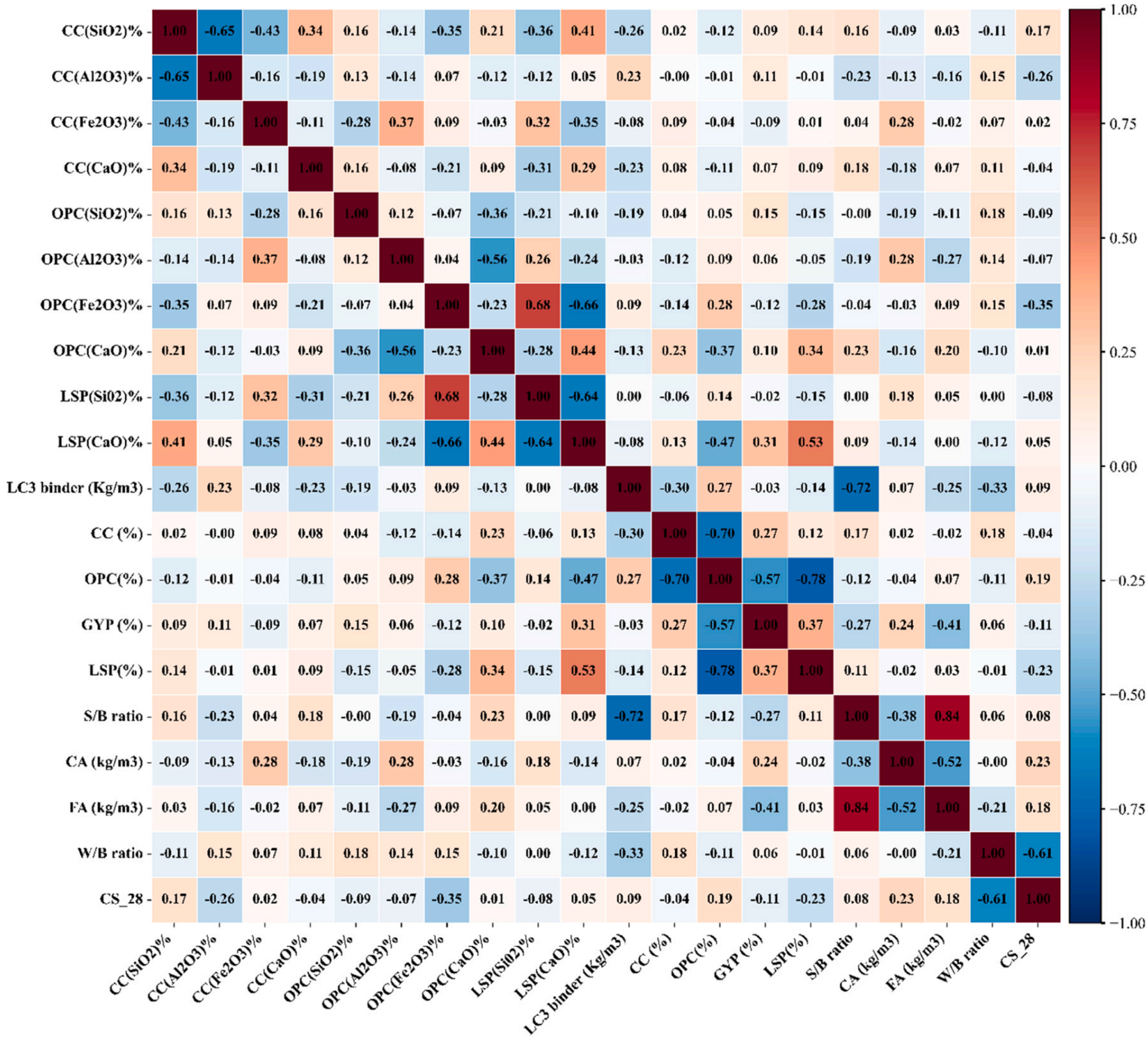

Fig. 2. Correlation between input and output parameters.

2.5. Density distribution

Fig. 3 density distribution plots show how the normalized values of CS (28 days) vary with the individual mix parameters, providing insight into the role of each feature in strength development. Indeed, mixes with higher LC^3 binder content are associated with increased strength, since their density peaks fall at the upper range of CS (28 days), confirming that adequate binder dosage is conducive to developing a dense and cohesive microstructure. In return, the W/B ratio follows an opposite trend; higher the W/B value, lower the strength density, emphasizing the negative impact of excess water on matrix porosity and thereby strength reduction. The distribution of OPC and CC contents overlaps but are balanced, indicating that the moderate clinker substitution with CC maintains strength when combined with optimal proportions of LSP and binder. The distribution of the CaO- and Al_2O_3-rich raw materials exhibit wider distributions, indicating involvement in the hydration reaction and formation of C-S-H and carboaluminates. A moderate peak is observed at the mean value of S/B ratio distribution, indicating that well-graded FA contributes to increased packing density and internal load transfer inside a composite. These distributions collectively illustrate that LC^3 concrete performance is determined from the joint adjustment of various interacting parameters, such as binder chemistry, aggregate proportion, and water control, therefore multivariate modeling and optimization approaches plays important role in predicting the mechanical performance of the concrete.

2.6. Preliminary experimental validation program

An experimental program was conducted to provide preliminary validation of the optimized mixture of LC^3 concrete obtained using the machine learning and GWO method. OPC, CC, LSP, and Gyp were used as binder materials. Natural fine aggregates (FA) and coarse

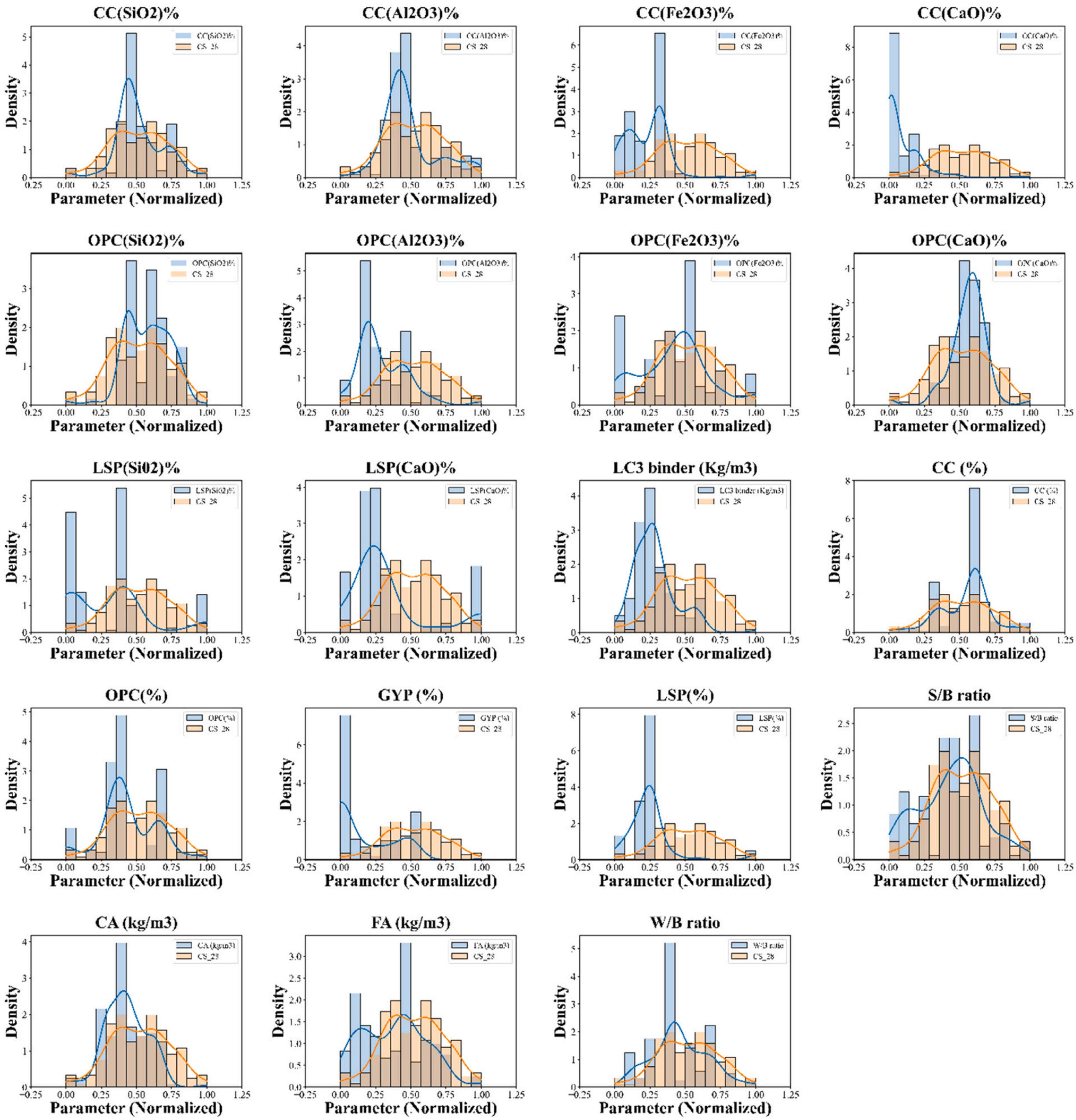

Fig. 3. Relationship between compressive strength and other features.

aggregates (CA) were used as the granular skeleton. Fig. 4 depicts the materials used in the experimental work.

The XRF method was used to determine the chemical composition of OPC, CC, and LSP. The oxide composition of the materials is shown in Table 3. Oxide compositions are SiO_2, Al_2O_3, Fe_2O_3, CaO, MgO, SO_3, P_2O_5 and K_2O, along with traces. To make sure the raw elements were appropriate for making LC^3 concrete, this test was carried out.

The chemical compositions confirm the suitability of the raw materials for LC^3 production. The experiment employed a mixture that was designed in accordance with the proportions that were optimized by the GWO algorithm. The optimized concrete mixture was prepared using a mixer. Initially, dry components including binder, FA, and CA, were mixed for 1 min to achieve a uniform distribution. Water was then added, and mixing was continued for 3 min. Finally, the mixture was mixed at a higher speed for an additional 1 min to improve its homogeneity. The total mixing time was 5 min. The fresh concrete was cast into $100 \times 100 \times 100$ mm cube molds. After casting, the specimens were covered with a plastic sheet to minimize moisture loss and were demoulded after 24 h. The specimens were then immersed in water at $25 \pm 2\,^{\circ}C$ until the designated testing age. As the specimens were fully immersed in water, relative humidity was not used as a curing parameter. For the preliminary validation, three cube specimens were tested at 28 days

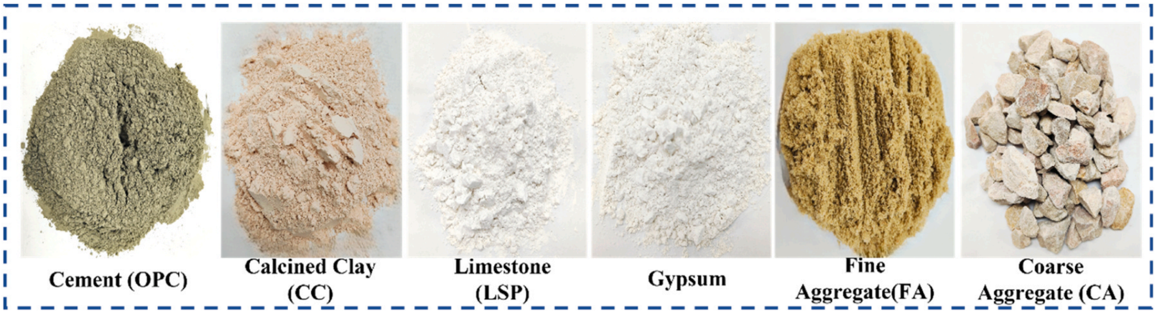

Fig. 4. Raw materials used in the study.

Table 3
Chemical composition of raw materials (wt%).

Composition	OPC, %	CC, %	LSP, %
SiO_2	16.02	59.45	14.40
Al_2O_3	3.63	28.65	-
Fe_2O_3	3.41	6.86	0.33
CaO	66.34	0.64	77.80
MgO	-	0.21	7.44
SO_3	3.73	-	-
K_2O	0.68	0.36	-
TiO_2	0.29	3.83	-
P_2O_5	0.29		

using a hydraulic compression testing machine. The compressive load was applied continuously at a constant rate of 1 kN/s until failure. The average compressive strength of the three specimens was used for comparison with the strength predicted by the CatBoost–GWO framework. The mixture's details are provided in Section 6.4.

3. Soft computing techniques

In this study, four ML algorithms, namely CatBoost, XGBoost, LightGBM, and Random Forest (RF), were used to model and predict 28-day CS of LC^3 concrete. The best algorithm were then combined with GWO algorithm to find optimum concrete mix.

CatBoost is a gradient-boosting decision tree algorithm developed by Yandex, which is distinguished by its ability to handle both categorical and numerical features with minimal preprocessing. Ordered boosting and symmetric tree techniques are used to prevent overfitting and it improves the predictive performance. In this study, CatBoost was chosen for its ability to identify complex non-linear relationships between LC^3 concrete mix parameters and strength properties [64,65].

Extreme Gradient Boosting (XGBoost) is a fast and efficient ML algorithm based on the gradient boosting method. XGBoost is an enhancement of the traditional gradient boosting method, where second-order information is used to prevent overfitting and achieve high prediction accuracy. Considering the success of this method in regression problems in various engineering and data science fields, XGBoost method was used to evaluate the boosting-based strength prediction in the LC^3 dataset [66].

RF is an ensemble learning algorithm that creates many decision trees from randomly selected samples of data. The model also selects a random subset of features at each split. The final prediction is achieved by averaging the results of all trees to reduce overfitting and improve generalization [67].

LightGBM is a fast gradient boosting tree approach developed around 2017. It uses histogram-based splits, along with leaf-wise growth with depth limits, for efficient training without compromising accuracy [68].

Since the present study was dealing with structured tabular data, tree-based ensemble models were selected as they are most suitable for such data and can also capture the nonlinear relationship between concrete mix parameters. Their successful applications to predicting concrete properties further justify their use on the present LC^3 dataset. However, emerging lightweight neural-network architectures provide alternative approaches for engineering prediction problems. For instance, a lightweight Kolmogorov–Arnold Network (KAN) based dual-objective optimization was used to predict the axial capacity of concrete-filled steel tube columns recently [69]. Such methods may provide a useful balance between prediction accuracy and computational efficiency. The present study did not include the development and/or application of KAN-based models; however, their comparison with ensemble models may be considered for future LC^3 research, especially given the availability of larger datasets.

GWO, a population-based metaheuristic algorithm inspired by the hierarchical leadership characteristic of gray wolves and their cooperative hunting behavior. It was first introduced by Mirjalili et al. (2014) and has since become a widely used optimization method in engineering and computational design [70]. The algorithm framework is based on social hierarchy of wolves in the pack, defined by alpha (α), beta (β), delta (δ), and omega (ω). The top three wolves - α, β, and δ - represent the best solution set and lead the rest of the pack in the searching process. The GWO algorithm is based on the wolves behavior when they hunt their prey; the wolves surround the prey, hunt, and then attack the prey through mathematical computation based on the location of the prey (solution set). The exploration and exploitation mechanisms of GWO can reduce the risk of premature convergence, although global optimality cannot be guaranteed. GWO was selected in this study because it has a simple structure, requires relatively few algorithm-specific parameters, and can be applied to bounded nonlinear optimization problems [71–74]. These characteristics make it suitable for searching the LC^3 mix-design space, where several mixture variables interact with each other. In this study, GWO was integrated with a CatBoost prediction model to carry out single-objective optimization, whose goal was to maximize the predicted strength of the LC^3 concrete. The GWO algorithm was used to vary the binder content, OPC %, CC%, LSP %, GYP% and W/B ratio to identify the optimal combination that would result in the maximum strength. The inclusion of GWO in this study helped to provide a data-driven method of concrete mix design optimization. It reduced the dependency on traditional trial-and-error laboratory methods while ensuring that the optimized LC^3 concrete mixes achieve both high performance and sustainability. Other metaheuristic algorithms have also been applied to ML-assisted engineering optimization, e.g., genetic algorithms (GA), particle swarm optimization (PSO), and differential evolution. The optimization algorithm's performance has been recently reported to be problem-dependent and to rely upon the type of ML model used and the nature of the concrete drying problem [75]. Therefore, the present study does not assume that GWO is superior to all other optimizers. GWO was selected as a simple and suitable search method for the present LC^3 mix-design problem. Future research should involve making a direct comparison between GWO and other optimization algorithms.

4. Hyperparameter optimization

Table 4 presents the optimized hyperparameters for all four ensemble algorithms through GridSearchCV with five-fold cross-validation. Each model's settings were optimized with a balance of prediction accuracy and generalization. XGBoost prefers deep ensembles with small learning rates and high regularization. On the other hand, CatBoost aims at efficiency through moderate depth and fast learning. A relatively deep structure with 85 estimators helped to maximize the reduction in variance in the Random Forest model. The LightGBM converged fast by using a high learning rate coupled with tree depth compactness so as not to compromise its computation efficiency at the cost of accuracy. Overall, the tuned parameters determined the base for valid estimations of compressive strength in LC^3 concrete.

5. Model evaluation matrices

Four significant parameters have been used to assess and evaluate the performance of the machine learning model. These include Root Mean Squared Error (RMSE), Mean Squared Error (MSE), Mean Absolute Error (MAE), and the Determination Coefficient (R^2). The coefficient of determination, denoted by R^2, measures the proportion of variation of the dependent variable that can be explained by the machine learning model. MAE measures the average magnitude of absolute errors between predicted and actual values, and

Table 4
Optimized hyperparameters of ML models.

ML Model	Hyperparameter	Value
CatBoost (CAT)	depth	5
	iterations	50
	l2_leaf_reg	3
	learning_rate	0.3
	random_seed	2
	subsample	0.9
XGBoost (XGB)	colsample_bytree	0.8
	gamma	0.1
	learning_rate	0.02
	max_depth	5
	min_child_weight	3
	n_estimators	1000
	reg_alpha	0.1
	reg_lambda	1
	subsample	1.0
RF	max_depth	30
	max_features	None
	min_samples_leaf	1
	min_samples_split	5
	n_estimators	85
	random_state	2
LightGBM	learning_rate	0.5
	max_depth	5
	n_estimators	25
	random_state	42
	reg_lambda	5
	subsample	0.4

MSE measures the squared errors average. RMSE, which is a square root of MSE, focuses more on large errors during the prediction process. The mathematical representation of these evaluation metrics is given by Eqs. (1)–(4).

$$R^2 = 1 - \frac{\sum_{i=1}^{n}(y_i - \widehat{y}_i)^2}{\sum_{i=1}^{n}(y_i - \overline{y}_i)^2} \tag{1}$$

$$MAE = \frac{1}{n}\sum_{i=1}^{n}|y_i - \widehat{y}_i| \tag{2}$$

$$MSE = \frac{1}{n}\sum_{i=1}^{n}(y_i - \widehat{y}_i)^2 \tag{3}$$

$$RMSE = \sqrt{\frac{1}{n}\sum_{i=1}^{n}(y_i - \widehat{y}_i)^2} \tag{4}$$

where (y ¯) is the mean of the actual values.

6. Results and discussions

6.1. Performance comparison of ML models

Predictive modeling was done by employing four ensemble-based ML algorithms: CatBoost, XGBoost, RF, and LightGBM. Table 5 summarizes the model's results. CatBoost algorithm outperformed the other three models, with a R^2 of 0.872, RMSE of 4.55 MPa, and MAE of 3.46 MPa on the test set. The best performance of CatBoost can be attributed to its ordered boosting method, that helps to reduce overfitting and effectively handles both numerical and categorical input variables.

Both XGBoost and Random Forest models presented R^2 values of approximately 0.84, indicating reliable generalization capability. Accuracy was slightly worse for LightGBM, with substantial underprediction in the higher strength levels. These results across the models indicate that boosting-based algorithms, especially CatBoost, perform better in detecting non-linear relationships between multiple mix parameters than bagging-based algorithms.

6.2. Actual vs predicted strength analysis

Fig. 5 demonstrated real vs. predicted scatter plots for the models, which illustrate the real vs. predicted values for the models. The points in the graphs should ideally lie along the 45-degree line. In the case of the CatBoost model, it is clear that the points are closely aligned with the 45-degree line, indicating that the model has the highest level of consistency in its predictions. Although the XGBoost model and the RF model also showed a high level of consistency in their predictions, the points did not lie as closely along the equality line as in the case of the CatBoost model. The LightGBM model showed a high level of dispersion in the points, which is in accordance with the slightly lower level of accuracy indicated in Table 5. The strong correlation and close alignment of the actual and projected data for CatBoost show the model's robustness in capturing the complex interplay of LC^3 mix parameters such as CC, LSP, and W/B ratio.

6.3. Taylor diagram analysis

Fig. 6 (Taylor diagram) compares models based on standard deviation (SD), correlation coefficient, and centered root-mean-square difference. CatBoost is the closest to the reference point, with the highest correlation (about 0.95) and the lowest centered RMS error; XGBoost and RF all perform well (correlation over 0.90), although LightGBM deviates more, indicating more error variance. Overall, the diagram supports the numerical results and highlights the advantage of gradient boosting methods for modeling complex nonlinear LC^3 concrete behavior.

6.4. Optimization by CatBoost-GWO

A hybrid GWO–CatBoost framework was used to maximize the compressive strength, where CatBoost predicted compressive

Table 5
Performance comparison of ML models.

Model	RMSE	MSE	MAE	R^2
CATBoost	4.5472	20.6769	3.4638	0.8721
XGBoost	5.0558	25.5609	3.7021	0.8419
Random Forest	5.0535	25.5380	3.7970	0.8421
LightGBM	5.1235	26.2500	4.1035	0.8377

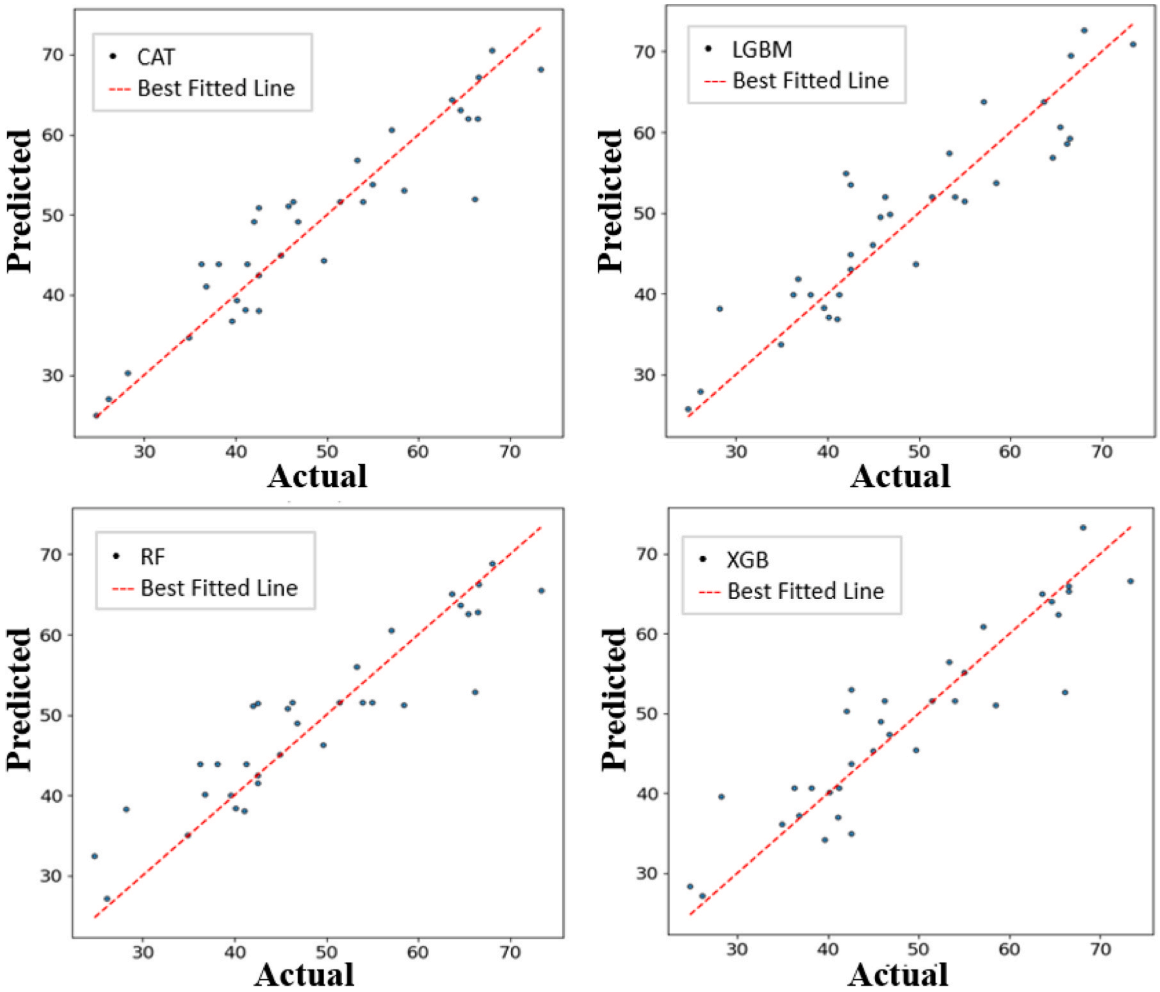

Fig. 5. Actual and predicted values of all ML models for the testing dataset.

strength and GWO searched for the best mix proportions. The optimization targeted only the practical variables that could be controlled in the laboratory: CC, OPC, GYP, and LSP contents (%, by binder), S/B ratio, CA, FA, and W/B ratio as shown in Table 6. The oxide compositions were not optimized because the available raw materials had fixed chemical compositions. It would be difficult in practice to obtain new materials with oxide compositions suggested by the optimizer. Therefore, the oxide-related inputs and other non-optimized features were fixed at the median values of the training dataset. This provided representative conditions for the optimization. GWO then performed a search of those variables that can be easily controlled when designing a concrete mix. This method also eliminated unrealistic changes in the material chemistry and minimized the number of optimization variables. However, the resulting optimum is conditional on the fixed chemistry and should not be considered universally optimal for all LC^3 raw-material sources. Furthermore, the model for CatBoost was trained with mixtures of different oxide compositions. The trained model will still be influenced by these variables if they are not fixed during GWO. Rather, optimization is done conditionally at a single representative chemistry with controllable mix variables varying. So, the optimized solution is the model solution for the chosen chemical conditions. Different fixed oxide compositions may lead to different optimal mix proportions and should therefore be examined in future studies. Lower-upper bounds were applied to all decision variables to ensure feasibility, and the binder fractions were renormalized so that OPC + CC + GYP + LSP added to 100% while remaining within individual limits. The objective (fitness) value was calculated as the CatBoost-predicted compressive strength minus a scaled boundary penalty:

$$\text{Objective} = \text{CS\_pred} - 0.05 \times \text{Penalty}$$

The penalty was applied to stop infeasible solutions, yet for maintaining the main optimization goal as compressive strength. Quadratic penalties were applied for solutions outside the bounds, linear penalties for solutions within 2% of the bounds. Further, the binder fractions were re-normalized to make them add up to 100%. This defined a direct binder composition limit. The number of wolves and iterations in GWO were slowly ramped up from 50 and 800–120 and 2200, respectively. The final setting was chosen since any further increase of the value did not significantly improve the objective value and only slightly change the optimized mix

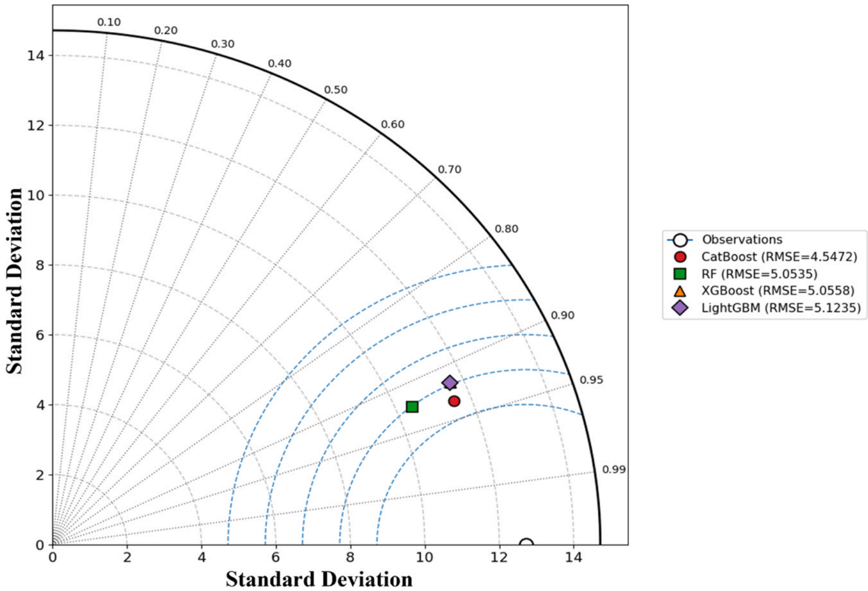

Fig. 6. Taylor diagram for ML models.

Table 6
Optimized mix design details for LC^3 concrete.

	Mix Details
Wolves & Iteration	Run: wolves= 120, iterations= 2200
CC(%)	34.680824
OPC(%)	54.750643
GYP(%)	0.087618
LSP(%)	10.480915
S/B ratio	2.389383
CA (kg/m^3)	996.20088
FA (kg/m^3)	821.591247
W/B ratio	0.390588
Predicted CS (MPa)	57.2055

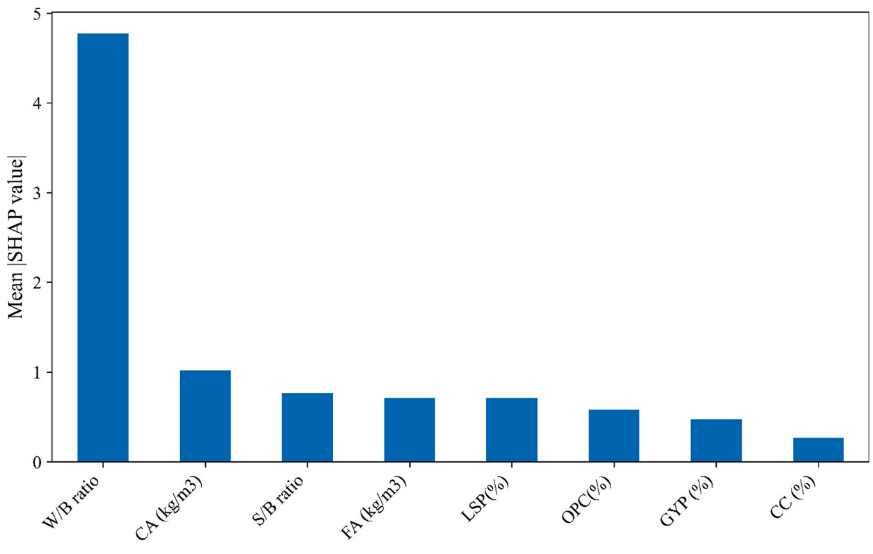

Fig. 7. Global feature importance based on mean absolute SHAP values for optimized LC^3 mix parameters.

proportions. No systematic sensitivity analysis of the penalty weight and various constraint-handling techniques was carried out, however. Thus, the reported optimum is the one achieved with the particular GWO parameters and constraint formulation.

6.5. Explainable machine learning analysis

From the SHAP analysis, Fig. 7 illustrates the global feature effects, while Table 7 reports the MeanAbsSHAP (overall importance) together with Corr(Value, SHAP) (directionality). The SHAP "Corr(Value, SHAP)" correlates feature values against that feature's SHAP contribution. A negative correlation means higher feature values generally reduce the predicted compressive strength (CS), while a positive correlation means higher values generally increase CS.

The most influential feature in the SHAP analysis is the W/B ratio, with a MeanAbsSHAP value of 4.77 compared to the second, CA, at value of 1.02. It also has a high negative direction (Corr(Value, SHAP) = −0.953). This outcome is physically sensible as it relates directly to the amount of water available against the binder, and has a big impact on capillary porosity and compressive strength. Additionally, mechanical properties of previous LC^3 systems have been reported to be strongly dependent on the W/B ratio [6].

However, the large difference between the SHAP importance of W/B and the other features should be interpreted with caution. SHAP importance reflects the behavior of the model learned from the set of data that is available, and is not a general material law. The literature-derived database comprises of mixtures from several material sources and experimental programs, with some material properties, like curing details and reactivity properties of calcined-clay, not fully represented by the model inputs. Hence, the high W/B importance could be due to its actual effect on the compressive strength as well as the design of the dataset used. Bias in the data sets and/or the unevenness in the representation of the data sets in the input cannot be ruled out. Additional testing with larger and more well-balanced LC^3 datasets is required to ascertain if the same degree of W/B dominance is retained. The following most influential variables have predominantly positive contributions. CA exhibits moderate positive directionality (MeanAbsSHAP = 1.02; Corr = +0.495), showing that higher CA generally increases CS. The S/B ratio is linked with CS (MeanAbsSHAP = 0.77; Corr = +0.681), representing that higher S/B tends to enhance the strength. The sand-to-binder ratio (S/B) affects packing density, interfacial transition zone quality, and stress distribution in concrete. An ideal S/B ratio improves particle packing while reducing internal voids. Improved packing reduces porosity and improves load transfer efficiency between paste and aggregates, leading to increased compressive strength. FA has a significant positive reliance (MeanAbsSHAP = 0.71; Corr = +0.786), which means that raising FA generally pushes CS upward depending on the other mix variables. LSP (%) is the main negative factor after W/B ratio (MeanAbsSHAP = 0.713; Corr = −0.735), suggesting that larger LSP content reduces projected CS. In LC^3 systems, limestone reacts with alumina present in CC to produce carbo-aluminate phases that help in refining the microstructure. However, this is only possible within an optimum proportion range. When there are more limestone and insufficient alumina, there is limited formation of additional strength and even increased porosity. Thus, increasing LSP percentages beyond the optimum range may result in decreased compressive strength due to binder dilution effects and decreased formation of strength-increasing hydrates. Overall, the explainability results indicate that the model primarily learns a strong strength sensitivity to W/B ratio (negative), with secondary strength gains linked to aggregate and proportioning variables (CA, S/B, FA), while higher LSP tends to penalize CS.

The SHAP beeswarm plot provides a view of SHAP distribution values for each and every feature across all data samples presented in Fig. 8. Each point on the graph represents a sample of a mix. The colors represent the magnitude of each feature value, where red indicates a high feature value and blue indicates a low feature value. With regard to W/B ratio, we see that all the red points are on the negative SHAP side, meaning that a high value for W/B results in lower strength. With regard to CA, S/B, and FA, we see that all the red points are on the positive SHAP side, meaning that a high value results in increased strength. With regard to LSP, we see that a high value results in a negative SHAP value. The SHAP beeswarm plot is a graphical representation of the results that we also found numerically in the Table 7.

6.6. Preliminary experimental validation

The optimized LC^3 concrete mix proposed by the CatBoost–Gray Wolf framework was subjected to preliminary experimental validation using the procedure described in Section 2.6. Three 100 mm cube specimens (n = 3) were tested at 28 days. The model predicted 28-day CS of 57.21 MPa, while the average measured strength from the three cubes was 51.54 MPa with a standard deviation of 0.21 MPa, as presented in Fig. 9. This gives a difference of 5.67 MPa, meaning the test result is 9.9% lower than the predicted

Table 7
SHAP-based feature importance and directionality analysis using MeanAbsSHAP and Corr(Value, SHAP).

Rank	Feature	MeanAbsSHAP	Corr(Value, SHAP)
1	W/B ratio	4.77	-0.95
2	CA (kg/m^3)	1.02	+ 0.495
3	S/B ratio	0.77	+ 0.681
4	FA (kg/m^3)	0.71	+ 0.786
5	LSP (%)	0.713	-0.735
6	LC^3 binder (kg/m^3)	0.623	+ 0.218
7	OPC (%)	0.582	+ 0.651
8	GYP (%)	0.477	+ 0.12
9	CC (%)	0.269	-0.388

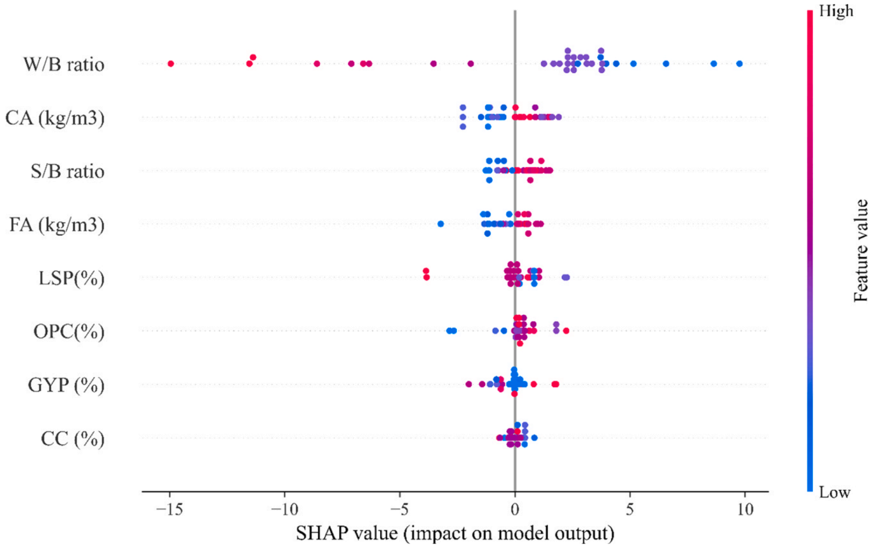

Fig. 8. SHAP beeswarm plot showing the distribution and directional impact of input features on predicted compressive strength.

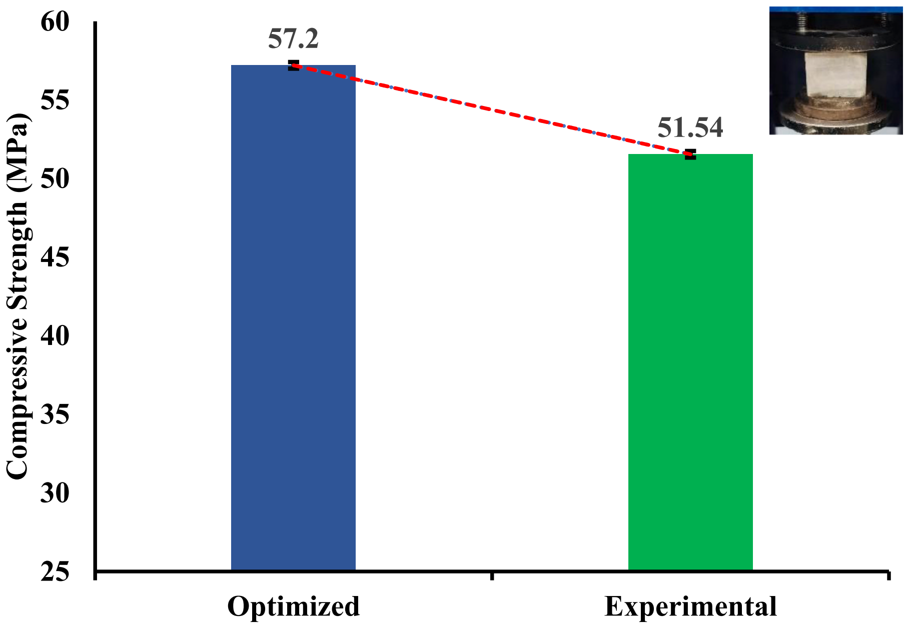

Fig. 9. Experimental vs optimized compressive strength result.

value.

The discrepancy in strength between the predicted and experimental values of 9.9% could be attributable to some degree of heterogeneity in the database and some material variability. Table 2 was compared with the optimized controllable mix variables, and it was observed that the variables are within the range of each and every variable in the compiled dataset. For instance, the optimum W/B value was 0.391 whereas the range of W/B in the database was 0.25–0.60. The optimized values of CC, OPC, LSP, S/B, CA, FA were also in their corresponding minimum and maximum range. Thus, the optimized values did not exceed the individual ranges represented in the database. However, this univariate comparison does not establish that the complete optimized combination lies within the multivariate training domain.

The prediction model was developed from different published studies and the experimental validation was carried out with one set of local materials and experimental conditions. CC reactivity, lime stone properties, cement chemistry, particle characteristics, mixing, compaction and curing conditions may influence the strength of LC^3. The model inputs do not fully reflect some of these factors. Some of these differences could be part of the reason there is a difference between the predicted strength and the actual one. This study did not include a detailed multivariate applicability-domain analysis, which may be necessary when implementing future studies. For new material sources, local calibration is recommended as well. Despite the observed difference, the measured strength of 51.54 MPa shows that the optimized mixture achieved a high 28-day compressive strength under the investigated laboratory conditions.

7. Limitations and future research

The proposed framework showed good predictive performance and was subjected to preliminary validated experimentally, but there are some limitations. These restrictions offer some directions for future research:

1. Dataset size: The final dataset contained 169 LC^3 concrete mixtures with 19 input features. The models might not be generalizable due to the smaller size of the dataset, variations in material properties, and experimental setup. The dataset should be extended with more experimental results in future studies. Alternatively, synthetic data augmentation methods (SDAMs) such as CTGAN can be explored if the synthetic data meets the physical and compositional requirements of LC^3 concrete [76].
2. Generalization to new materials: the experimental data were tested against one set of local materials, whereas the data in the model were collected from various literature sources. Additional testing with other raw materials is required. A smaller experimental data set could be used to adapt a literature-trained model to local materials, by means of transfer learning [77]. For new material systems, a formal applicability-domain assessment should be conducted before application of the model.
3. Optimization scope: Optimizing to obtain the maximum compressive strength of 28 days. The solution optimization with regards to sensitivity against the penalty weight and a variety of constraint-handling strategies were not explored systematically. Further research is needed to assess the robustness of the optimization process and to expand the framework to include the incorporation of multiple objectives such as workability, durability, cost and embodied CO_2.
4. Practical implementation: The following framework is not yet implemented in a practical software tool. The prediction, interpretation of SHAP and optimization procedures could be combined in an interactive platform for future work [78]. This would enable the ability to set material properties and design constraints, and provide feasible LC^3 mix recommendations with predicted performance.

8. Conclusions

This study established a data-driven approach for LC^3 concrete mix design by combining ML prediction, metaheuristic optimization, and experimental validation. The method was trained using a literature-derived LC^3 concrete database and then used to identify a high-strength optimum mix using GWO. The optimized design was subsequently subjected to preliminary experimental validation using 28-day compressive strength testing.

1. A compiled dataset of LC^3 concrete mixes was used to train ML models for predicting CS of 28-days. In terms of accuracy and generalization, CatBoost outperformed other models.
2. CatBoost was combined with a single-objective metaheuristic optimizer (GWO) to find an optimum mix and a predicted 28-day strength of 57.21 MPa.
3. SHAP interpretability analysis indicates that compressive strength is primarily determined by the W/B ratio, aggregate proportions and binder composition. This behavior is consistent with established physical understanding of concrete strength development and supports the interpretability of the model.
4. Preliminary experimental validation was performed by testing three 100 mm cubes under standard water curing. The average compressive strength after 28 days was 51.54 MPa, which had a 9.9% difference from the predicted value. The observed difference may partly result from variations between the literature-derived training data and the local materials used for experimental testing.
5. The prediction-test difference shows the susceptibility of LC^3 systems to CC reactivity, LSP fineness/purity, additive compatibility, and curing condition. It is recommended to include a small local calibration set when deploying the framework with new material sources; future transfer-learning approaches may provide an efficient way to perform such local adaptation.

CRediT authorship contribution statement

Md Rakib Hossain: Writing – original draft, Methodology, Investigation, Formal analysis, Data curation. **Amin Al-Fakih:** Writing – review & editing, Supervision, Resources, Methodology, Funding acquisition, Conceptualization. **Jawad Khalil:** Writing – review & editing, Validation, Formal analysis. **Abdullah Alshahrani:** Writing – review & editing. **Fahd Saeed Alakbari:** Writing – review & editing, Validation. **Ayman Almutlaqah:** Writing – review & editing, Funding acquisition.

Disclosure

This manuscript has been edited with the AI-assisted technology for grammar correction and stylistic improvements. All content, intellectual contributions, and final interpretations remain the responsibility of the authors, who have thoroughly reviewed and approved the final version of the manuscript.

Funding

The authors gratefully acknowledge the support provided by the Deanship of Research, King Fahd University of Petroleum & Minerals (KFUPM), under Grant EC26104.

Declaration of Competing Interest

The authors declare that they have no known competing financial interests or personal relationships that could have appeared to influence the work reported in this paper.

Acknowledgments

The authors would like to express their sincere gratitude to the Department of Civil and Environmental Engineering, King Fahd University of Petroleum & Minerals, for their continued support.

In addition, the authors are thankful to the Deanship of Graduate Studies and Scientific Research at Najran University for funding this work under the Consortium Funding Program grant code (NU/CPL/SERC/14/3767–2).

Data availability

Data will be made available on request.

References

[1] K. Xiao, H. Zhang, S. Wei, C. Zhu, J. He, S. Zhu, X. Yang, Prediction of compressive strength of high-performance concrete based on multiple machine learning models, Front. Mater. 12 (2025), https://doi.org/10.3389/fmats.2025.1698248.
[2] S. Humagain, G. Shrestha, M.K. Madhavan, P.K. Sarker, Hydration, soundness, and strength of low carbon LC3 mortar using waste brick powder as a source of calcined clay, Materials 18 (2025), https://doi.org/10.3390/ma18153697.
[3] Y. Fang, C. Yang, H. Zeng, J. Yang, H. Zhang, Y. Gu, H. Chu, L. Jiang, Synergistic effects of limestone calcined clay cement on alkalinity, mechanical performance, and vegetative compatibility of ecological concrete, Sci. Rep. 16 (2026), https://doi.org/10.1038/s41598-026-38329-6.
[4] A. Boanada -Fuchs, U. Heierli, K. ScrivenerHarmonizing environmental goals and housing needs, 2024.
[5] I. Kafodya, D. Basuroy, J.M. Marangu, G. Kululanga, R. Maddalena, V.I. Novelli, Mechanical performance and physico-chemical properties of limestone calcined clay cement (LC3) in Malawi, Buildings 13 (2023), https://doi.org/10.3390/buildings13030740.
[6] Y. Yu, M. Yang, C. Wan, L. Lin, Mechanical, workability, economic and environmental properties of concrete with limestone calcined clay cement and recycled aggregates, Sci. Rep. 15 (2025), https://doi.org/10.1038/s41598-025-97539-6.
[7] Y. Dhandapani, T. Sakthivel, M. Santhanam, R. Gettu, R.G. Pillai, Mechanical properties and durability performance of concretes with limestone calcined clay cement (LC3), Cem. Concr. Res. 107 (2018) 136–151, https://doi.org/10.1016/j.cemconres.2018.02.005.
[8] M. Sharma, S. Bishnoi, F. Martirena, K. Scrivener, Limestone calcined clay cement and concrete: A state-of-the-art review, Cem. Concr. Res. 149 (2021), https://doi.org/10.1016/j.cemconres.2021.106564.
[9] Y. Hu, L. Xiong, Y. Yan, G. Geng, Performance of limestone calcined clay cement (LC3) incorporating low-grade marine clay, Case Stud. Constr. Mater. 20 (2024), https://doi.org/10.1016/j.cscm.2024.e03283.
[10] Z. Feng, J. Zhao, G. Huang, W.V. Liu, Influence of water-to-binder ratios on the performance of limestone calcined clay cement-based paste for mining applications, Green Smart Min. Eng. 1 (2024) 262–272, https://doi.org/10.1016/j.gsme.2024.08.001.
[11] S.C. Sapkota, A. Shrestha, W. Tang, Metaheuristic-optimized machine learning models for accurate prediction of limestone calcined clay cement (LC3) compressive strength, Case Stud. Constr. Mater. 23 (2025), https://doi.org/10.1016/j.cscm.2025.e05303.
[12] D.S.A. Jubori, A.B. Nabilah, N.A. Safiee, A.H. Alias, N.A.M. Nasir, Machine learning technique for the prediction of blended concrete compressive strength, KSCE J. Civil. Eng. 28 (2024) 817–835, https://doi.org/10.1007/s12205-024-0854-5.
[13] T. Han, B.K. Aylas-Paredes, J. Huang, A. Goel, N. Neithalath, A. Kumar, On the prediction of the mechanical properties of limestone calcined clay cement: a random forest approach tailored to cement chemistry, Minerals 13 (2023), https://doi.org/10.3390/min13101261.
[14] X. Chen, W. Chen, Z. Li, P. Zhang, A hybrid prediction and multi-objective optimization framework for limestone calcined clay cement concrete mixture design, Sci. Rep. 15 (2025), https://doi.org/10.1038/s41598-025-05288-3.
[15] Z. Liu, E. Li, J. Zhou, Predictive modeling and interpretation of LC3-ECC compressive strength using XGBoost and gene expression programming, Mater. Today Commun. 49 (2025), https://doi.org/10.1016/j.mtcomm.2025.113842.
[16] O. Canbek, Q. Xu, Y. Mei, N.R. Washburn, K.E. Kurtis, Predicting the rheology of limestone calcined clay cements (LC3): linking composition and hydration kinetics to yield stress through Machine Learning, Cem. Concr. Res. 160 (2022), https://doi.org/10.1016/j.cemconres.2022.106925.
[17] T. Bansal, V. Talakokula, P. Sathujoda, Machine learning-based monitoring and predicting the compressive strength of different blended cementitious systems using embedded piezo-sensor data, Measurement 205 (2022), https://doi.org/10.1016/j.measurement.2022.112204.
[18] Y. Zhang, Z. Wang, J. Liu, Y. Li, Z. Huang, X. Yu, A metaheuristic-driven categorical boosting framework with interpretability for high-precision prediction of mechanical properties in corroded reinforced concrete beams, Eng. Appl. Artif. Intell. 163 (2026), https://doi.org/10.1016/j.engappai.2025.112804.
[19] M.R. Hossain, M. Sajid, J.U. Mamun, E. El-Wajih, J. Khalil, A. Al-Fakih, Machine-learning-based prediction of the compressive strength of limestone calcined clay cement (LC3) mortar, Arab. J. Sci. Eng. (2026), https://doi.org/10.1007/s13369-026-11162-9.
[20] S.C. Sapkota, A. Shrestha, W. Tang, Metaheuristic-optimized machine learning models for accurate prediction of limestone calcined clay cement (LC3) compressive strength, Case Stud. Constr. Mater. 23 (2025), https://doi.org/10.1016/j.cscm.2025.e05303.
[21] J.M. Marangu, Prediction of compressive strength of calcined clay based cement mortars using support vector machine and artificial neural network techniques, J. Sustain. Constr. Mater. Technol. 5 (2020) 392–398, https://doi.org/10.29187/jscmt.2020.43.
[22] B. Hilloulin, V.Q. Tran, Interpretable machine learning model for autogenous shrinkage prediction of low-carbon cementitious materials, Constr. Build. Mater. 396 (2023), https://doi.org/10.1016/j.conbuildmat.2023.132343.
[23] S. Bhattacherjee, S. Jain, M. Santhanam, Harnessing the adsorption mechanism of pce-based sp and dispersing agent with limestone calcined clay cement-based systems to enhance workability retention, 2024. https://www.researchgate.net/publication/384763204.
[24] S. Mukherjee, R. Kumar, M. Behera, A. Goyal, M.R. Rahman, Rheology, mechanical properties and microstructure characterization of limestone calcined clay cement (LC3) incorporated sustainable lightweight self-compacting concrete, Dev. Built Environ. 21 (2025), https://doi.org/10.1016/j.dibe.2025.100601.

[25] B. Rath, Praveenkumar T.R, K.S. Dhami, P. Paramasivam, M. Yusuf, Sustainable LC3 concrete in the circular economy: assessment of mechanical, microstructural, and durability characteristics with surkhi, metakaolin, nano-silica, and M-sand blended concrete, Glob. Chall. 9 (2025), https://doi.org/10.1002/gch2.202500026.
[26] A. Kijjanon, T. Sumranwanich, W. Saengsoy, S. Tangtermsirikul, Chloride penetration resistance, electrical resistivity, and compressive strength of concrete with calcined kaolinite clay, fly ash, and limestone powder, J. Mater. Civil. Eng. 35 (2023), https://doi.org/10.1061/(asce)mt.1943-5533.0004643.
[27] W. Du, L. Jiang, Q. Liu, W. Chen, Q. Ding, Study on the influence of thermoplastic microcapsules on the sulfate resistance and self-healing performance of limestone calcined clay cement concrete, Molecules 29 (2024), https://doi.org/10.3390/molecules29204797.
[28] V. Shah, S. Bishnoi, Carbonation resistance of cements containing supplementary cementitious materials and its relation to various parameters of concrete, Constr. Build. Mater. 178 (2018) 219–232, https://doi.org/10.1016/j.conbuildmat.2018.05.162.
[29] V. Shah, A. Parashar, G. Mishra, S. Medepalli, S. Krishnan, S. Bishnoi, Influence of cement replacement by limestone calcined clay pozzolan on the engineering properties of mortar and concrete, Adv. Cem. Res. 32 (2020) 101–111, https://doi.org/10.1680/jadcr.18.00073.
[30] L. Chen, K. Zheng, T. Xia, G. Long, Mechanical property, sorptivity and microstructure of steam-cured concrete incorporated with the combination of metakaolin-limestone, Case Stud. Constr. Mater. 11 (2019), https://doi.org/10.1016/j.cscm.2019.e00267.
[31] M. Santhanam, Y. Dhandapani, R. Gettu, R.G. Pillai, T. Sakthivel, S. Rengaraju, S. Rathnarajan, F. Suma, A.S. Basavaraja, S. Prakasan, N. NairSummary of 4-years of research at IIT Madras on concrete with limestone calcined clay cement (LC3), 2019. https://www.researchgate.net/publication/331948577.
[32] N. Nair, K. Mohammed Haneefa, M. Santhanam, R. Gettu, A study on fresh properties of limestone calcined clay blended cementitious systems, Constr. Build. Mater. 254 (2020), https://doi.org/10.1016/j.conbuildmat.2020.119326.
[33] A.A. Ramezanianpour, A. Zolfagharnasab, A. Hossein, Y. Yaraghi, A.M. Ramezanianpour, A.Y. Yaraghi, F. Bahman-Zadeh, Mechanical properties and durability of concretes containing calcined clays and limestone powder, 2020. https://www.researchgate.net/publication/372217420.
[34] Z. yu Huang, Y. shuo Huang, W. yu Liao, N. xu Han, Y. wu Zhou, F. Xing, T. bo Sui, B. Wang, H. yan Ma, Development of limestone calcined clay cement concrete in South China and its bond behavior with steel reinforcement, J. Zhejiang Univ. Sci. A 21 (2020) 892–907, https://doi.org/10.1631/jzus.A2000163.
[35] P. Desai, A. Kalathingal, Fresh and hardened properties of pastes and concretes with lc3 and its economic viability: Indian ready mix industry perspective. RILEM Bookseries, Springer, 2020, pp. 821–832, https://doi.org/10.1007/978-981-15-2806-4_92.
[36] F. Avet, K. Scrivener, Study of concrete made of limestone calcined clay cements (LC3). RILEM Bookseries, Springer, 2020, pp. 257–261, https://doi.org/10.1007/978-981-15-2806-4_29.
[37] K.D. Musbau, J.T. Kolawole, A.J. Babafemi, O.B. Olalusi, Comparative performance of limestone calcined clay and limestone calcined laterite blended cement concrete, Clean. Eng. Technol. 4 (2021), https://doi.org/10.1016/j.clet.2021.100264.
[38] K. Purushotham Reddy, B.D.V. Chandra Mohan Rao, M. Janardhan Yadav, P. Swamy Naga Ratna Giri, Comparative studies on LC3based concrete with OPC & PPC based concretes. Mater. Today Proc., Elsevier Ltd, 2020, pp. 2368–2372, https://doi.org/10.1016/j.matpr.2021.01.833.
[39] S. Kavya Sree, B.D.V. Chandra Mohan Rao, M.J. Yadav, P. Swamy Naga Ratna Giri, Experimental studies on mechanical and durability characteristics of lc 3 concrete, IOP Conf. Ser. Mater. Sci. Eng. 1091 (2021) 012075, https://doi.org/10.1088/1757-899x/1091/1/012075.
[40] J. Yu, D.K. Mishra, C. Hu, C.K.Y. Leung, S.P. Shah, Mechanical, environmental and economic performance of sustainable Grade 45 concrete with ultrahigh-volume limestone-calcined clay (LCC), Resour. Conserv. Recycl. 175 (2021), https://doi.org/10.1016/j.resconrec.2021.105846.
[41] B.V. Vaasudevaa, Y. Dhandapani, M. Santhanam, Performance evaluation of limestone-calcined clay (LC2) combination as a cement substitute in concrete systems subjected to short-term heat curing, Constr. Build. Mater. 302 (2021), https://doi.org/10.1016/j.conbuildmat.2021.124121.
[42] S.M. Gunjal, B. Kondraivendhan, High temperature impact on calcined clay-limestone cement concrete (LC3), Mater. Today Proc. 61 (2022) 386–391, https://doi.org/10.1016/j.matpr.2021.10.300.
[43] S. Pradhan, A. Chang Boon Poh, S. Qian, Impact of service life and system boundaries on life cycle assessment of sustainable concrete mixes, J. Clean. Prod. 342 (2022), https://doi.org/10.1016/j.jclepro.2022.130847.
[44] K. Ram, M. Flegar, M. Serdar, K. Scrivener, Influence of low- to medium-kaolinite clay on the durability of limestone calcined clay cement (LC3) concrete, Materials 16 (2023), https://doi.org/10.3390/ma16010374.
[45] M. Guo, G. Gong, Y. Yue, F. Xing, Y. Zhou, B. Hu, Performance evaluation of recycled aggregate concrete incorporating limestone calcined clay cement (LC3), J. Clean. Prod. 366 (2022), https://doi.org/10.1016/j.jclepro.2022.132820.
[46] S. Bhavani, M.L.V. Prasad, A low carbon cement (LC3) as a sustainable material in high strength concrete: green concrete, Mater. De. Constr. 73 (2023), https://doi.org/10.3989/mc.2023.355123.
[47] M.D. Sheikh, T. Jamil, T. Ayub, A.U.R. Khan, S.M. Bilal, C. Hu, Comparative study on LC3-50 with OPC concrete using raw materials from Pakistan, Adv. Mater. Sci. Eng. 2023 (2023), https://doi.org/10.1155/2023/5503670.
[48] S. Nasiri, R. Madandoust, M.M. Ranjbar, Investigating the calcination temperature and grinding time of calcined clay on the mechanical properties and durability of LC3 concrete, Infrastructure 8 (2023), https://doi.org/10.3390/infrastructures8100139.
[49] A.S. Basavaraj, H. Muni, Y. Dhandapani, R. Gettu, M. Santhanam, Limestone-calcined clay (LC2) as a supplementary cementitious material for concrete, RILEM Tech. Lett. 8 (2023) 12–22, https://doi.org/10.21809/rilemtechlett.2023.172.
[50] A. Sharma, A.B.D. Roy, P.P. Bansal, Post-heating evaluation of fibre reinforced concrete with LC3 binder as replacement to OPC, Constr. Build. Mater. 407 (2023), https://doi.org/10.1016/j.conbuildmat.2023.133603.
[51] A.M. Salman, M.A. Akinpelu, I.T. Yahaya, H.M. Salami, Workability and strengths of ternary cementitious concrete incorporating calcined clay and limestone powder, in: Mater. Today Proc., Elsevier Ltd, 2023, pp. 51–58, https://doi.org/10.1016/j.matpr.2023.02.249.
[52] M. Goudarzi, F. Moodi, A.M. Ramezanianpour, A. Zolfagharnasab, A.A. Ramezanianpour, Assessing the risk of ASR in LC3 binders based on low-grade calcined clay, Constr. Build. Mater. 428 (2024), https://doi.org/10.1016/j.conbuildmat.2024.136302.
[53] E.S. Leo, M.G. Alexander, H. Beushausen, Compressive strength and durability performance of limestone calcined clay cement concrete made from selected African raw materials, Constr. Build. Mater. 438 (2024), https://doi.org/10.1016/j.conbuildmat.2024.137012.
[54] M. Pellerano, G. Samson, C. Patapy, A. Calviac, M. Cyr, Development of self-compacting low-carbon concretes for precast industry, Constr. Build. Mater. 457 (2024), https://doi.org/10.1016/j.conbuildmat.2024.139114.
[55] S.M. Gunjal, S.D. Turkane, S.V. Patankar, B. Kondraivendhan, Effect of magnesium sulphate and sulphuric acid attack on limestone calcined clay cement concrete, Mater. Today Proc. (2023), https://doi.org/10.1016/j.matpr.2023.03.488.
[56] K. Venkataraman, P.R.K. Rajkumar, Study on performance, mechanical behaviour and microstructural characteristics of eco-friendly limestone calcined clay cement (LC3) concrete with GGBS – a sustainable approach, Int. J. Sustain. Constr. Eng. Technol. 15 (2024) 203–220, https://doi.org/10.30880/ijscet.2024.15.04.015.
[57] C. Venkatesh, V. Mallikarjuna, G.M. Rao, S.K. Patil, B.N. kiran, M.K. Yashwanth, C. Venkata Siva Rama Prasad, G. Sree Lakshmi Devi, Synergistic effects of graphene oxide and limestone calcined clay cement on mechanical properties and durability of concrete, J. Build. Pathol. Rehabil. 9 (2024), https://doi.org/10.1007/s41024-024-00470-y.
[58] X. Huang, Z. Jiao, F. Xing, L. Sui, B. Hu, Y. Zhou, Performance assessment of LC3 concrete structures considering life-cycle cost and environmental impacts, J. Clean. Prod. 436 (2024), https://doi.org/10.1016/j.jclepro.2023.140380.
[59] K.S. Sreekeshava, S. Kolathayar, N. Vinod, C. Menon, Recent advances in structural engineering, 2024.
[60] X. Huang, Z. Huang, Y. Zhou, R. Hu, B. Hu, Life cycle assessment and cost analysis of LC3 concrete considering sustainability and uncertainty, J. Build. Eng. 102 (2025), https://doi.org/10.1016/j.jobe.2025.111960.
[61] P. Wang, H. Lai, W. Li, L. Ke, H. Wu, W. Li, C.K.Y. Leung, Mechanical properties and environmental impact assessments of GFRP rebar reinforced limestone calcinated clay cement (LC3) concrete, Constr. Build. Mater. 472 (2025), https://doi.org/10.1016/j.conbuildmat.2025.140788.
[62] M.S.H. Khan, Q.D. Nguyen, A. Castel, Carbonation of limestone calcined clay cement concrete. RILEM Bookseries, Springer Netherlands, 2018, pp. 238–243, https://doi.org/10.1007/978-94-024-1207-9_38.

[63] Z. Huang, Y. Huang, L. Sui, N. Han, F. Xing, T. Sui, Bond behavior between limestone calcined clay cement (LC3) concrete and steel rebar. in: RILEM Bookseries, Springer, 2020, pp. 563–570, https://doi.org/10.1007/978-981-15-2806-4_63.
[64] C.S. Kulkarni, Advancing gradient boosting: a comprehensive evaluation of the catboost algorithm for predictive modeling, J. Artif. Intell. Mach. Learn. Data Sci. 1 (2022) 54–57, https://doi.org/10.51219/jaimld/chinmay-shripad-kulkarni/29.
[65] A.V. Dorogush, V. Ershov, A. GulinCatBoost: gradient boosting with categorical features support, 2018. http://arxiv.org/abs/1810.11363..
[66] T. Chen, C. GuestrinXGBoost: a scalable tree boosting system, In: Proceedings of the ACM SIGKDD International Conference on Knowledge Discovery and Data Mining, Association for Computing Machinery, 2016: pp. 785–794. https://doi.org/10.1145/2939672.2939785.
[67] G. Biau, E. Scornet, A random forest guided tour, Test 25 (2016) 197–227, https://doi.org/10.1007/s11749-016-0481-7.
[68] G. Ke, Q. Meng, T. Finley, T. Wang, W. Chen, W. Ma, Q. Ye, T.-Y. Liu, LightGBM: A Highly Efficient Gradient Boosting Decision Tree, n.d. https://github.com/Microsoft/LightGBM.
[69] X. Kong, Y. Fan, J. Liu, M. Xi, Y. Zhang, Y. Yu, Lightweight Kolmogorov-Arnold Network with dual-objective optimization for axial capacity prediction of square coal gangue concrete-filled steel tube stub columns based on finite element simulation, Eng. Appl. Artif. Intell. 176 (2026), https://doi.org/10.1016/j.engappai.2026.114843.
[70] S. Mirjalili, S.M. Mirjalili, A. Lewis, Grey wolf optimizer, Adv. Eng. Softw. 69 (2014) 46–61, https://doi.org/10.1016/j.advengsoft.2013.12.007.
[71] N.M. Hatta, A.M. Zain, R. Sallehuddin, Z. Shayfull, Y. Yusoff, Recent studies on optimisation method of Grey Wolf Optimiser (GWO): a review (2014–2017), Artif. Intell. Rev. 52 (2019) 2651–2683, https://doi.org/10.1007/s10462-018-9634-2.
[72] A.A. Heidari, R. Ali Abbaspour, H. Chen, Efficient boosted grey wolf optimizers for global search and kernel extreme learning machine training, Appl. Soft Comput. J. 81 (2019), https://doi.org/10.1016/j.asoc.2019.105521.
[73] Y. Liu, A. As'arry, M.K. Hassan, A.A. Hairuddin, H. Mohamad, Review of the grey wolf optimization algorithm: variants and applications, Neural Comput. Appl. 36 (2024) 2713–2735, https://doi.org/10.1007/s00521-023-09202-8.
[74] H. Li, H. Kang, J. Li, Y. Pang, G. Sun, S. Liang, Single-objective and multi-objective mixed-variable grey wolf optimizer for joint feature selection and classifier parameter tuning, Appl. Soft Comput. 165 (2024), https://doi.org/10.1016/j.asoc.2024.112121.
[75] D. Liang, X. Xue, J. Liu, Y. Cui, Z. Sun, Y. Zhang, T. Zhang, L. Xu, Matching metaheuristics to machine learning for concrete drying shrinkage prediction toward cost-effective mix design, Dev. Built Environ. 27 (2026), https://doi.org/10.1016/j.dibe.2026.100964.
[76] J. Liu, S. Wang, K. Chen, K. Wang, Y. Fan, Q. Wang, Synthetic data augmentation and Integrated prediction framework for low-carbon recycled concrete: leveraging CTGAN and multiple ML models stacking, J. Clean. Prod. 543 (2026), https://doi.org/10.1016/j.jclepro.2026.147599.
[77] C. Wang, W. Chu, J. Liu, Y. Zhao, F. Liu, Y. Zhang, M. Rashidi, Y. Yu, Unified axial capacity prediction of FRP-confined concrete across natural and recycled aggregate systems using a Kolmogorov-Arnold Networks based cross-domain transfer-learning framework, Structures 90 (2026), https://doi.org/10.1016/j.istruc.2026.112255.
[78] Haoming Wang, Yuzhuo Zhang, Jinlong Liu, Yuqing Zhao, Ruoqi He, Shuzhi Xu, Weiwei Wang, Xuetao Lyu, Data-driven reliability-based optimization framework for concrete-encased steel composite columns toward cost-effective design: methodology and interactive tool, Adv. Struct. Eng. (2026) 13694332261447524, https://doi.org/10.1177/13694332261447524.